Advances in Materials Technology for Fossil Power Plants
Proceedings from the Eighth International Conference
October 11–14, 2016, Albufeira, Algarve, Portugal
https://doi.org/10.31399/asm.cp.am-epri-2016p0478

STRUCTURAL CHANGES IN P92-TYPE MARTENSITIC STEEL DURING CREEP AT 600°C

A. Fedoseeva, I.Nikitin, V. Dudko*, N. Dudova, R. Kaibyshev
Belgorod State University, Pobeda 85, 308015 Belgorod, Russia

ABSTRACT

Structural changes in P92-type steel after creep at temperature of 600°C under a stress of 140 MPa were investigated. The steel was solution treated at 1050°C and tempered at 780°C. The structure in the grip portion of the crept specimen changed scarcely after creep exposure for 6876 h. In contrast, the structural changes in the gage and neck sections were characterized by transformation of the tempered martensite lath structure into relatively coarse subgrain structure. The formation of a well-defined subgrain structure in the gage and neck sections was accompanied by the coarsening of $M_{23}C_6$ carbides and precipitations of Laves phase during creep. Mechanisms of grain boundary pinning by precipitates are discussed.

INTRODUCTION

Grade 9Cr-2W-VNbB-type steel is an appropriate material for boilers and tubes of fossil power plants with working temperature of 600°C [1,2]. The high creep resistance of these high-chromium steels is associated with a tempered martensite lath structure (TMLS) consisting of prior austenite grains (PAG), packets, blocks, laths and containing a high density of dislocations and a dispersion of secondary phase particles. $M_{23}C_6$-type carbides and MX carbonitrides precipitate along boundaries and within ferritic matrix, respectively, during tempering, and particles of Fe_2(W,Mo) Laves phase precipitate at boundaries under creep conditions [1-7]. A P92-type steel is alloyed by substitutional alloying elements, such as W and Mo, to provide a high solid-solution strengthening and reduced diffusion rate, that gives a significant contribution to strengthening of TMLS under creep conditions, and, therefore, provides high creep resistance of this steel [1,3-6]. These elements affect a dispersion of carbides and carbonitrides, which hinder boundary migration and impede reactions between dislocations and subgrain boundaries [1,7]. Instability of TMLS under creep is considered to be the main reason for loss of creep resistance [1,3,5]. Coarsening of boundary $M_{23}C_6$ carbides and Laves phase takes place under long-term aging and creep conditions. The aim of present work is to investigate the structural changes in P92-type steel upon creep at 600°C.

MATERIAL AND METHODIC

P92-type steel with the chemical composition (in wt.%) of Fe_{bal}-0.1C-0.17Si-0.54Mn-8.75Cr-0.51Mo-1.6W-0.23V-0.07Nb-0.04N-0.003B was subjected to normalizing at 1050°C for 0.5 h and tempering at 780°C for 3 h. Cylindrical specimens with a gauge length of 100 mm and a diameter of 10 mm were tested until rupture at 600°C under an applied stress of 142 MPa using an ATS2330 lever arm machines. Microstructural characterization was performed in the grip, gage and neck portions of ruptured specimen using a JEM-2100 transmission electron microscope (TEM) equipped with an INCA energy dispersive X-ray spectroscope. The lath/subgrain sizes

were evaluated on TEM micrographs by the linear intercept method including all clearly visible (sub)boundaries. The dislocation densities were estimated by counting the individual dislocations in the grain/subgrain interiors per unit area on at least six arbitrarily selected typical TEM images for each data point. The mean size of the secondary phase particles was evaluated on TEM micrographs. The precipitates were identified by chemical composition and diffraction pattern analysis. Other details of structural characterization and specimen preparation were reported previously [3-5,8,9]. Equilibrium fractions of phases were calculated by the Thermo-Calc software using the TCFE7 database.

RESULTS

Microstructure after normalizing and tempering

Microstructure of steel studied after normalizing at 1050°C and tempering at 780°C is presented in Fig. 1, and structural parameters are summarized in Table 1. The average size of prior austenite grains (PAG) is ~20 μm. The higher tempering temperature (780°C) in comparison with standard tempering temperature (750°C) provides the formation of subgrain structure, mainly. On the other hand, the high dislocation density of ~10^{14} m^{-2} is observed within ferritic matrix.

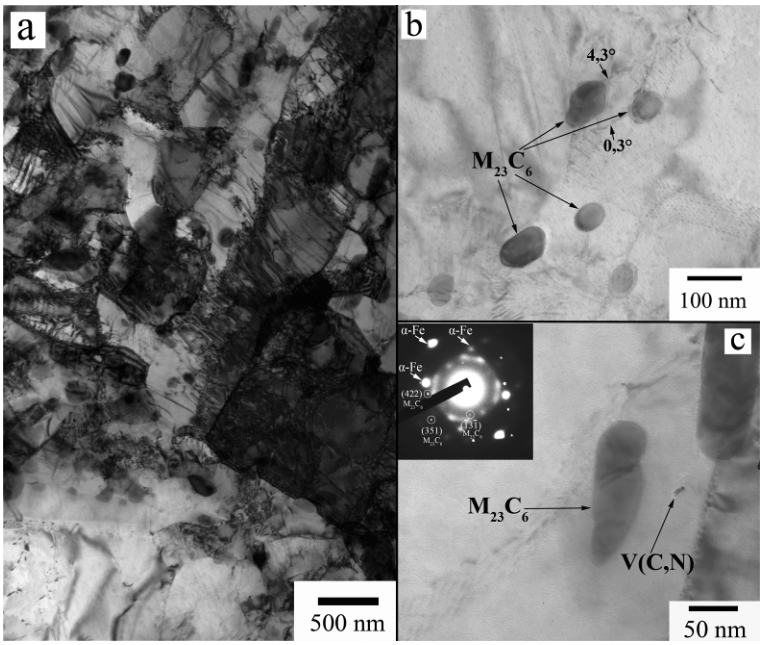

Figure 1: TEM micrographs of the P92-type steel after normalizing and tempering at 780°C: the numbers on (b) indicate the misorientation of subgrains, on which $M_{23}C_6$ carbides are located.

Table 1: Structural parameters of steel normalized and tempered at 780°C.

D_{PAG}, μm	$D_{subgrains}$, μm	$\rho_{\perp} \times 10^{14}$, m^{-2}	d_{M23C6}, nm	d_{MX}, nm
20±2	0.46±0.15	2.5±1	73±20	17±3

The boundaries of PAGs and subgrains are decorated by nanoscale $M_{23}C_6$ carbides. The mean size of $M_{23}C_6$ carbides is 73 nm after tempering at 780°C. Fine MX carbonitrides with plate-like shape precipitate within ferritic matrix. No separation of MX carbonitrides on V-rich and Nb-rich particles is observed. The mean size of MX carbonitrides is 17 nm.

Creep properties

Creep strain vs time and creep rate vs. time/strain curves at 600°C and nominal stress of 142 MPa are shown in Fig. 2. These curves are typical for 9%Cr martensitic steels containing a dispersion of secondary phase carbides and carbonitrides [1,4-7].

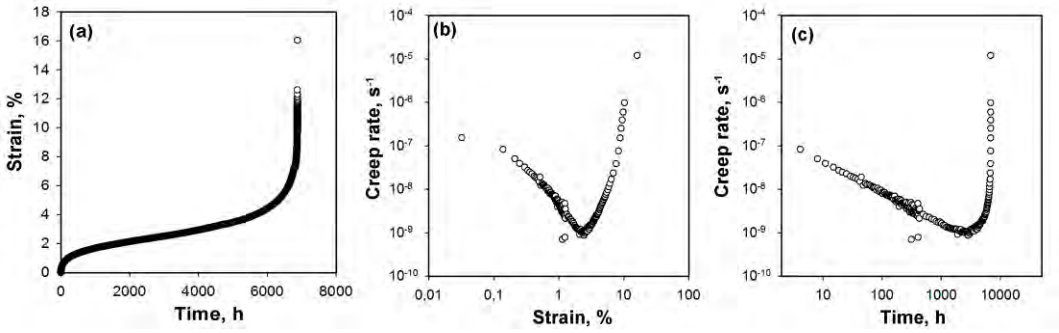

Figure 2: Creep curves of steel studied upon creep at 600°C, 142 MPa.

At an applied stress of 142 MPa, the extended transient stage is observed; creep rate slows down to the minimum value with increasing strain. Poor-defined steady state flow could be distinguished. Minimum creep rate of ~ 10^{-9} s^{-1} is approached at strain ~ 2-3% for ~ 3 000 h. Time to rupture at 600°C under a stress of 140 MPa is 6 876 h. Note that tertiary creep stage has one well-defined stage zone in contrast with 3%Co-containing P92-type steel [5,9].

Crept microstructure

Crept microstructures of the steels are shown in Fig. 3, and structural parameters are summarized in Table 2.

Table 2: Structural parameters of P92 steel after creep test at 600°C under an applied stress of 142 MPa.

Section	D_{PAG}, μm	D_{subgr}, μm	$\rho_{\perp} \times 10^{14}$, m^{-2}	$D_{particles}$, nm			
				$M_{23}C_6$	Laves	VX	NbX
Neck	20±2	0.73±0.1	0.6±0.1	170±15	200±20	52±5	100±10
Gage	20±2	0.68±0.1	2.0±1.0	170±15	220±20	55±5	65±3
Grip	20±2	0.51±0.1	2.0±1.0	115±12	210±10	55±5	24±3

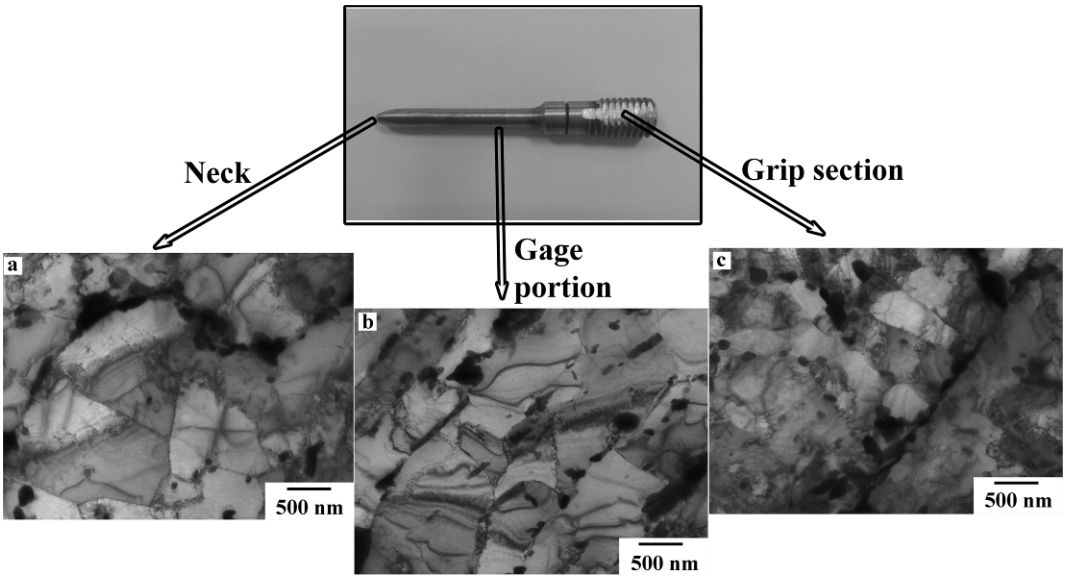

Figure 3: Microstructures of steels studied from different sections of sample: (a) in the neck and (b) in the gage portion (600°C, 142 MPa); (c) in the grip section (600°C, 6876 h).

It is seen that creep induces recovery and polygonization processes. However, no dynamic recrystallization was revealed. The long-term exposure at temperature of 600°C provides no evolution of subgrain structure (Fig.3c), while creep leads subgrain growth up to 0.65-0.75 μm (Fig. 3a and b, Table 2). High dislocation density remains within subgrains in the grip and gage portions, while in the neck the drop in dislocation density to ~10^{13} m^{-2} (Table 2) was found.
Chemical compositions of $M_{23}C_6$ carbides, the Laves phase and MX carbonitrides after long-term aging and creep are shown in Table 3.

Table 3: Chemical composition of second phases after aging and creep (at.%).

Phases	***Cr***	***Fe***	***W***	***Mo***	***V***	***Nb***
Long-term aging at 600°C for 6876 h (the grip section)						
$M_{23}C_6$	69.15	23.15	–	4.96	3.19	–
V-rich MX	18.22	7.56	–	–	61.31	12.85
Nb-rich MX	13.29	11.49	–	–	–	75.23
Laves phase	15.10	41.81	26.26	11.46	3.23	–
Creep, 600°C, 140 MPa (the gage portion)						
$M_{23}C_6$	66.73	24.01	–	5.20	2.51	–
V-rich MX	16.59	6.17	–	–	63.45	15.36
Nb-rich MX	13.85	6.17	–	–	6.70	73.40
Laves phase	14.95	41.70	27.06	12.75	3.30	–
Creep, 600°C, 140 MPa (the neck)						
$M_{23}C_6$	70.10	23.02	–	4.28	2.77	–
V-rich MX	16.00	3.56	–	–	67.83	12.15
Nb-rich MX	5.15	–	–	–	4.53	91.52
Laves phase	13.21	39.29	34.27	13.10	–	–

It is seen that chemical compositions of different phases are similar in different sections of sample. $M_{23}C_6$ carbides consist of 65-70 at.% Cr, 20-25% Fe, 5% Mo and 3% V. No W and Nb in $M_{23}C_6$ carbides have been observed. After creep test and long-term aging, there is a well-defined two-phase separation of MX carbonitrides into Nb- and V-rich dispersoids that are clearly distinguishable by morphology and chemical composition [1,10]. Nb-rich MX particles containing traces of V, Cr and Fe appear after long-term aging and creep (Table 3). V-rich MX particles are enriched by Cr and Nb. Laves phase particles contain 40-50 at.% (W+Mo) and 50-40% (Fe+Cr). The W/Mo ratio in the Laves phase particles is 2-2.5. The Laves phase particles precipitate at PAG and subgrain boundaries like $M_{23}C_6$ carbides under long-term aging and creep. These particles exhibit irregular shape and their size of ~200 nm is nearly the same in all sections (Table 2). Therefore, no strain-induced coarsening of Laves phase takes place. Strain-induced coarsening of $M_{23}C_6$ carbides occurs. $M_{23}C_6$ carbides grow up to 170 nm in the gage portion and neck of the sample, whereas in the grip section the size of $M_{23}C_6$ carbides is insignificantly higher than that in the tempered condition.

After creep and long-term aging the two-phase separation of MX carbonitrides to V-rich and Nb-rich particles appears. Nb-rich particles with a round shape and a mean size of ~24 nm and 100 nm precipitate in the grip and neck sections, respectively, that is indicative of strong strain-induced coarsening of Nb-rich MX carbonitrides. The size of V-rich particles increases from 17 nm to ~50 nm after long-term aging and creep test. Therefore no strain-induced coarsening of V-rich particles occurs, while significant Ostwald ripening of these particles takes place under static conditions (Table 2).

DISCUSSION

Two driving forces may be involved in subgrain coarsening. One of them is driving force originated from stored free lattice dislocations and second one is driving force attributed to subboundary energy [11,12]. Driving force due to stored dislocations is negligible because after creep test dislocations are homogeneously distributed in ferritic matrix. No difference in dislocation density in neighbor subgrains leads to negligible driving force due to stored dislocations. Driving force originated from low-angle boundary (LAB) energy can be evaluated as [11]:

$$P_{LAB} = \frac{2\gamma}{r} = \frac{2\gamma}{\alpha D} \tag{1}$$

where r is radius of curvature of subgrains (μm), which is proportional to grain/subgrain size D, α is constant.

The retarding force (Zener drag) exerted by the particles, which are randomly distributed in ferritic matrix (MX carbonitrides), depends on the size d and the volume fraction F_v of particles as [5,8,9,11,12]:

$$P_z = 3\gamma \frac{F_v}{d} \tag{2}$$

where γ is surface energy per unit area of the subgrain boundary. So, particles exerting the retarding force must prevent the growth of subgrain structure.

Pinning pressure from boundary $M_{23}C_6$ carbides and the Laves phase particles can be evaluated as:

$$P_B = \frac{\gamma F_{vB} D}{d^2} \tag{3}$$

where D represents the size of structural elements, i.e., the subgrain size. The volume fractions F_{vB} of boundary particles were calculated taking into account the boundary particle density β shown in Table 4 from the following relationship [8,9,12]:

$$\frac{F_{vB_i}}{F_{vB_0}} = \frac{D_0}{D_i} \cdot \frac{\beta_i}{\beta_0} \cdot \frac{d_i^2}{d_0^2} \quad (4)$$

where F_{vB0}, D_0, β_0, and d_0 are the parameters for the $M_{23}C_6$ carbides in the tempered state and for the Laves phase particles after short-term creep test (600°C, 200 MPa), and F_{vBi}, D_i, β_i, and d_i are the same parameters after the creep test.

Table 4 demonstrates the volume fractions of the second phases in steel, particle density at subgrain boundaries and Zener drags exerted by them calculated according to Eq. 2 and 3. It was suggested that MX carbonitrides are homogeneously distributed within ferritic matrix, while $M_{23}C_6$ carbides and the Laves phase particles are located on subgrain boundaries.

Table 4: Volume fractions of second phases at 600°C calculated by Thermo-Calc and Zener drag pressures exerted by second phase particles for the steel studied.

Section	*Volume fraction of particles, Fv, %*			*Particle density at subgrain boundaries, μm^{-2}*			*Zener drag pressure, MPa*		
	$M_{23}C_6$	*Laves*	*MX*	*Total*	*$M_{23}C_6$*	*Laves*	*$M_{23}C_6$*	*Laves*	*MX*
Neck	1.91	1.65	0.25	2.43	1.61	0.82	0.063	0.02	0.02
Gage				2.80	1.72	1.08	0,067	0.02	0.02
Grip				3.09	2.45	0.64	0.096	0.03	0.02

It is seen that $M_{23}C_6$ carbides have the highest contribution in total retarding forces in each section of sample studied (Table 4). Retarding forces originated from the Laves phase particles and MX carbonitrides are less than from $M_{23}C_6$ carbides in the steel.

An equilibrium subgrain size which may be achieved during polygonization can be estimated on the assumption of the driving and retarding forces are in a balance as follows:

$$D = \frac{2\gamma}{\alpha \sum (P_z + P_b)} \quad (5)$$

where α=4 [12]. The total retarding force that depends on the volume fraction and the mean size of particles affects the value of equilibrium subgrain size. The calculated values of subgrain size in the steel studied in comparison with the experimental values are presented in Table 5. It is seen that experimental subgrain size in P92-type steel reaches its equilibrium value, estimated by Eq. 5, that confirms the development of polygonization under creep.

On the other hand, the subgrain size depends on the applied stress under creep condition and can be estimated as:

$$D_\infty = 10\frac{Gb}{\sigma} \quad (6)$$

where G is a shear modulus, MPa, b is Burgers' vector, σ is an applied stress.

Table 5: Calculated and experimental values of subgrain size.

Section	D, μm (calculated by Eq. 5)	D_∞, μm (calculated by Eq. 6)	D, μm (exp. value)
Neck	0,74	1.1	0.73±0.1
Gage	0.72		0.68±0.1
Grip	0.52		0.51±0.1

Growth of subgrain size up to the strain-induced equilibrium value by Eq. 6 indicates the completeness of dynamic recovery and polygonization processes. However, experimental subgrain size in P92-type steel does not reach its equilibrium value, estimated by Eq. 6. So, the

subgrain size in steel studied during creep and long-term aging is determined only by balance between driving and retarding forces.

CONCLUSIONS

The microstructures of a P92-type steel tempered at 780°C and crept at 600°C under an applied stress of 142 MPa were studied. The main results can be summarized as follows.

1) Tempering at 780°C leads to formation of subgrain structure instead of TMLS with a mean subgrain size of 0.4 μm. $M_{23}C_6$-type particles with an average size of 73 nm precipitated on various interfaces including subgrain boundaries. MX-type particles with a mean size of 17 nm precipitated homogeneously throughout the ferritic matrix.
2) The structural changes were related to a gradual growth of ferrite subgrains. The mean sizes of subgrains were 0.5 and 0.7 μm in the grip section and the gage/neck portion, respectively.
3) The growth of subgrains during long-term aging and creep were determined by a coarsening of $M_{23}C_6$ carbides, the Laves phase particles and MX carbonitrides.

ACKNOWLEDGMENTS

The study was financially supported by the Russian Science Foundation, under grant No. 14-29-00173. The authors are grateful to the staff of the Joint Research Center, Belgorod State University, for their assistance with instrumental analysis.

REFERENCES

[1] Abe F. *et al,* Creep resistant steels, Woodhead Publishing in Materials (Cambridge, 2008), 678 p.
[2] Kern, T.-U., Staubli, M., Scarlin, B., "The European efforts in material development for 650°C USC power plants - COST522," *ISIJ International,* Vol. 42, Issue 12 SPEC. (2002), pp. 1515-1519.
[3] Kaybyshev, R.O., Skorobogatykh, V.N., Shchenkova, I.A., "New Martensitic Steels for Fossil Power Plant: Creep Resistance," *The Physics of Metals and Metallography*, Vol. 109 (2010), pp. 186–200.
[4] Kipelova, A., Odnobokova, M., Belyakov, A., Kaibyshev, R., "Effect of Co on creep behavior of a P911 steel," *Metall. Mater. Trans. A,* Vol. 44A, (2013), pp. 577-583.
[5] Dudova, N., Plotnikova, A., Molodov, D., Belyakov, A., Kaibyshev, R., "Structural changes of tempered martensitic 9%Cr-2%W-3%Co steel during creep at 650°C," *Mat. Sci. Eng. A,* Vol. 534, (2012), pp. 632-639.
[6] Abe, F., "Analysis of creep rates of tempered martensitic 9%Cr steel based on microstructure evolution," *Mater. Sci. Eng. A,* Vol. 510–511, (2009), pp. 64–69.
[7] Kostka, A., Tak, K.-G., Hellmig, R.J., Estrin, Y., Eggeler, G., "On the contribution of carbides and micrograin boundaries to the creep strength of tempered martensite ferritic steels," *Acta Materialia,* Vol. 55, (2007), pp. 539–550.
[8] Dudko, V., Belyakov, A., Molodov, D., Kaibyshev, R., "Microstructure Evolution and Pinning of Boundaries by Precipitates in a 9 pct Cr Heat Resistant Steel during Creep," *Metall. Mater. Trans. A*, Vol. 44A, (2013), pp. 162-172.
[9] Fedoseeva, A., Dudova, N., Kaibyshev, R., "Creep Strength Breakdown and Microstructure Evolution in a 3%Co Modified P92 Steel," *Mater. Sci. Eng. A*, Vol. 654, (2016), pp. 1-12.

[10] Suzuki, K., Kumai, Sh., Toda, Y., Kushima, H., Kimura, K., "Two-phase separation of primary MX carbonitride during tempering in creep resistant 9Cr1MoVNb steel," *ISIJ Intern.,* Vol. 43, (2003), pp. 1089–1094.
[11] Humphreys, F.J. et al, Recrystallization, Related Annealing Phenomena. Second ed., Elsevier (Oxford, 2004), 605 p.
[12] Kipelova, A., Kaibyshev, R.O., Belyakov, A., Molodov, D., "Microstructure evolution in a 3%Co modified P911 heat resistant steel under tempering and creep conditions," *Mater. Sci. Eng. A,* Vol. 528, (2011), pp. 1280–1286.